Thermocapillary and Arc Phenomena in Stainless Steel Welding

The influence of thermocapillary convection on weld shape is investigated for the gas tungsten arc process

BY S. W. PIERCE, P. BURGARDT AND D. L. OLSON

ABSTRACT. This investigation characterized the effects of power level and Gaussian heat source size on thermocapillary-induced weld shape and estimated the relative influence of various possible arc phenomena in determining weld shape. Welds made with the GTAW process were compared with similar ones made with a conduction-mode EBW process and the differences were related to arc effects.

Evidence of thermocapillary flow was readily apparent in both the GTA welds and the conduction-mode EB welds and was qualitatively similar in both. The similarity between the results obtained with the two processes serves to demonstrate that thermocapillary convection is the dominant factor in heat-to-heat weld shape variability. However, a simple one-to-one correspondence between welds produced with the two processes does not exist. Especially at high power, the EB welds showed stronger thermocapillary convection than the GTA welds.

One important arc factor that limits thermocapillary flow in arc welds appears to be an increase in arc size with arc length and arc current. A non-Gaussian arc power distribution in GTAW seems to be most important in limiting the fluid flow. Apparently, the arc power distribution is more nearly rectangular in shape for an argon gas arc. At higher currents, above 200 A, plasma shear force may also be an important contributor to weld shape development. The conduction-mode EB welds demonstrate that thermocapillary flow reversal probably does not occur in welds made with a simple Gaussian heat source. The complex shape behavior is likely a result of an arc effect such as plasma shear.

S. W. PIERCE and D. L. OLSON are with Colorado School of Mines, Golden, Colo. P. BURGARDT is with Los Alamos National Laboratory, Los Alamos, N.Mex.

Introduction

It is presently accepted that much of the weld shape variability observed in mechanized gas tungsten arc welding (GTAW) of stainless steel is linked to small variations in impurity, or trace element, concentration from one heat of material to another. Heiple and Roper (Ref. 1) proposed that thermocapillary convection (surface tension driven fluid flow — Marangoni effect) is primarily responsible for the weld shape variations, and that very small changes in material composition (especially of certain surface-active elements such as sulfur) will significantly affect the thermocapillary flow. Figure 1 illustrates a typical heat-to-heat GTA weld shape variation observed in Type 304 stainless steel. The weld shape is often characterized by the weld depth-to-width ratio (D/W), as determined from a transverse metallographic section of the weld. The GTA welds shown in Fig. 1A and 1B have D/W values of 0.22 and 0.47, respectively. Most of this weld shape difference is attributable to the sulfur content of the materials (about 10 ppm for the low D/W material and about 150 ppm for the high D/W material). Thermocapillary convection has been widely accepted as the primary mechanism of heat-to-heat weld pool shape variations, but it is recognized that other convection-and arc-related phenomena are also important in determining GTA weld shape (Ref. 2).

KEY WORDS

GTAW
EB
Arc Weld
Stainless Steel
Thermocapillary Flow
Weld Shape
Gaussian Power
Type 304
Maragoni Effect

Considerable computational and experimental works (Refs. 3–11) have demonstrated that GTA weld shape may also be influenced by several interrelated arc phenomena. The major arc phenomenon thought to influence weld shape is a result of electromagnetic (Lorentz) force in the weld pool and in the arc. The Lorentz force creates an inward flow in the weld pool, which tends to produce deeper weld penetration. Lorentz forces also create an inward pressure in the plasma of the arc that produces a gas flow down along and then away from the electrode. This flow in the plasma gas produces weld pool surface deformation and gas-shear-induced outward fluid flow in the weld metal. Depending on the relative magnitude of surface deformation and the shear-induced flow, the arc phenomena may promote deeper or shallower weld penetration. Actual weld shape is dependent on the interplay of normal conduction, thermocapillary

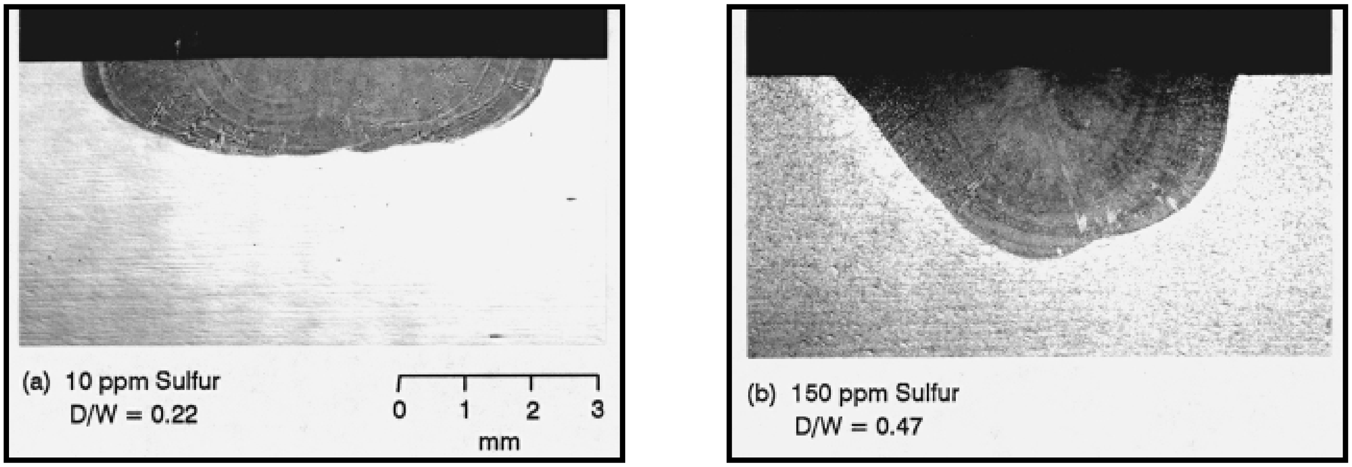

Fig. 1 — Weld shapes obtained with the GTA process of the two heats of material used in this study. A — The low-sulfur (10 ppm) material; B — the high-sulfur (150 ppm) material.

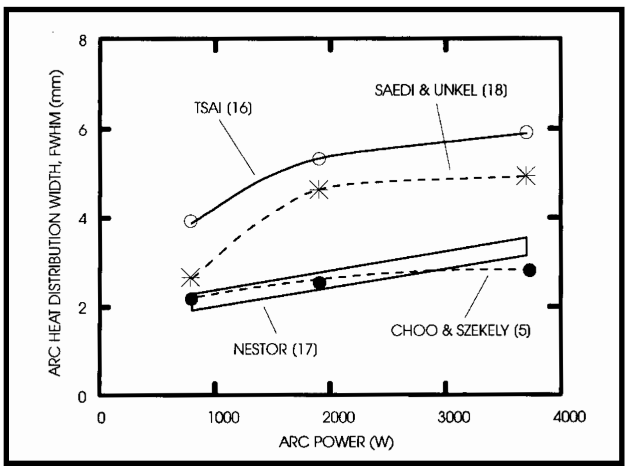

Fig. 2 — Measured arc heat distribution width (FWHM) vs. GTAW arc power level.

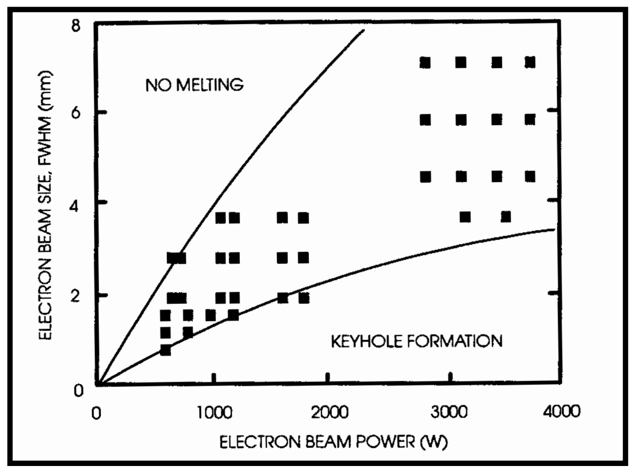

Fig. 3 — The EB weld matrix to regions delineating onset of melting and the onset of keyhole formation.

flow and the various arc factors. The relative strength and influence of these phenomena are dependent on the power level and the power distribution of the heat source.

An additional possible explanation for complex weld shape behavior is the thermocapillary flow reversal proposed by Burgardt and Heiple (Ref. 12). Burgardt and Heiple proposed that the complex weld shape changes that occur with increasing input energy density (higher arc power, slower travel speed, shorter arc length, etc.) in materials with deep penetration behavior may occur when the liquid metal under the heat source becomes very hot. If the metal immediately under the arc exceeds a surface temperature of about 2000°C, this material will have a lower surface tension than the metal toward the weld pool edge. In this case, there is a region where the inward thermocapillary flow (the normal flow for a material containing surface-active elements) is interrupted and the weld shape will tend toward a lower weld depth-to-width ratio. This is the phenomenon we refer to as thermocapillary flow reversal.

The purpose of the present investigation was to determine the relative importance of the various arc and fluid flow phenomena in producing GTA weld shape. The various arc influences are difficult to measure directly. Therefore, an indirect method for determining these effects is needed. To estimate the relative importance of the possible arc factors in determining weld shape, GTA welds were made and compared with similar welds made with a nonarc process (electron beam welding). Note that experiments of this general nature have been done previously (Refs. 13 and 14) and showed that thermocapillary flow in nonarc conduction mode welds (laser and electron beam welds) is qualitatively similar to that in arc welds. However, no attempt was made to quantify the various effects in those studies.

The nonarc process used here was conduction-mode electron beam welding (EBW). "Conduction mode" refers to welds made with sufficiently low power density that a keyhole is not formed and the beam power is deposited on the work top surface. In this case, weld shape is determined by normal conduction and convection processes. EBW is well suited to this study since the process has nearly ideal properties: 1) Welds are made in a high vacuum, 2) negligible current is used (less than about 30 mA), 3) the beam power enters the workpiece with high efficiency and reproducibility, 4) beam power can be adjusted to match arc welding values, 5) the beam size can be readily adjusted over a wide range and 6) the actual beam size and shape can be measured by relatively simple techniques.

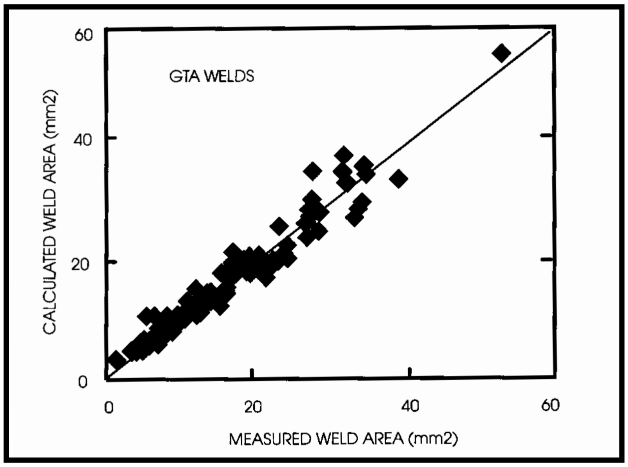

Fig. 4 — Experimental GTA weld cross-sectional area vs. calculated weld area showing the validity of Equation 3.

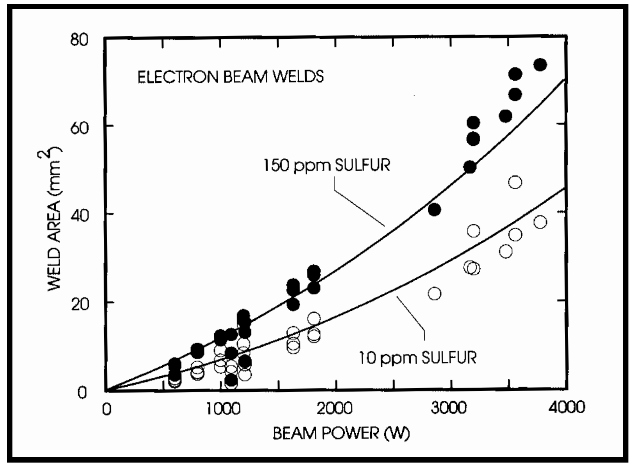

Fig. 5 — Electron beam weld cross-sectional area vs. beam power for the two heats of material. The lines illustrate the validity of Equation 4.

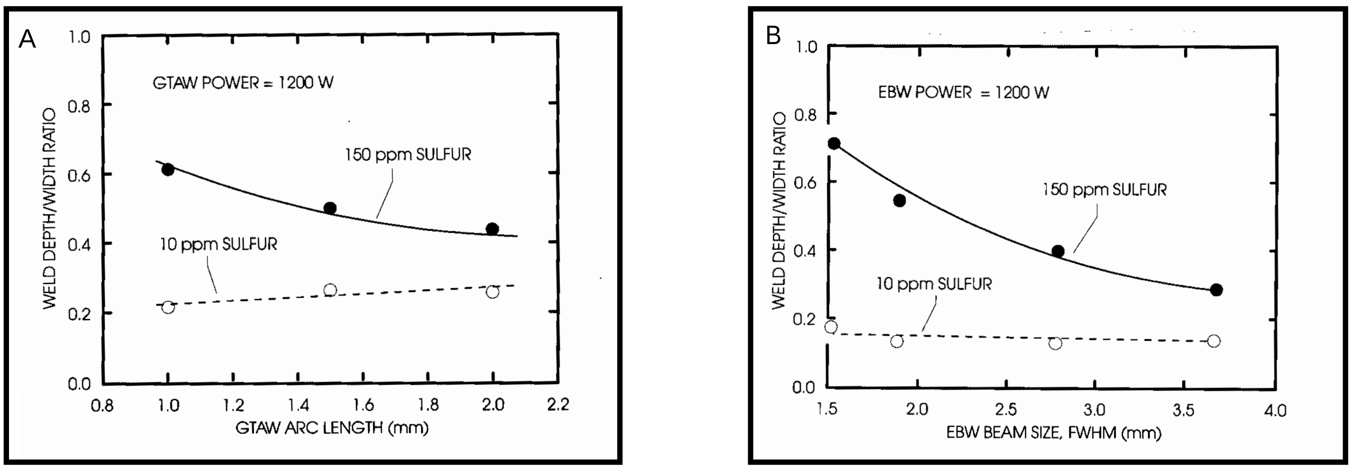

Fig. 6 — Weld D/W ratios for GTA and similar EB welds made on low-and high-sulfur material. A — GTA weld D/W ratios v. arc length; B — EB weld D/W ratios vs. beam size.

Beam size and power density are varied in a measurable and reproducible fashion by adjusting the degree of beam defocus. By using EBW, it is possible to produce welds made with identical travel speed, input power and comparable power input distribution to that achieved in GTA welding but without the various arc factors (such as Lorentz forces and anode spot wandering) being present.

Experimental Procedures

Beam and Arc Power Distributions

Measurement of the electron beam power distribution was accomplished for this study using a modified Faraday cup (MFC) apparatus (Ref. 15). The particular device used in this investigation utilizes a long slit to sample the electron beam current density as the beam is swept across the aperture. In this way, a profile of the beam was determined in a direction lateral to the welding direction. A long slit type of aperture was used here because a slit is sufficiently rugged to withstand full beam power for a considerable time and because data analysis is particularly simple in this situation. Unfortunately, beam shape data is lost in the direction parallel to the slit (for this work, the slit direction was parallel to the direction of travel). The beam shape in the direction of weld travel is not thought to be particularly important to the transverse weld geometry. Therefore, the long slit beam shape data are adequate for the purposes of this study.

Beam profiles were obtained for this study over the wide range of beam power and beam defocus conditions that were used. In all cases, the beam is nearly Gaussian in shape and is described by

$$J = \frac{I}{2\pi\sigma^2}\exp\left(\frac{-r^2}{2\sigma^2}\right) \quad (1)$$

where J is the beam current density, I is the total beam current; σ is the width of the distribution and r is the radial distance from the center of the beam point. Measurement of beam size consists of determining the value of σ that describes the beam for a particular set of welding conditions. Note, in this paper the beam size is generally quoted as the power distribution full width at half-maximum (FWHM). FWHM is related to σ by

$$\text{FWHM} = 2.36\ \sigma. \quad (2)$$

Electron beam size data were obtained for all accelerating voltage, beam current and defocus values used in this work. These measurements showed that the electron beam size is about σ = 0.1 mm at sharp

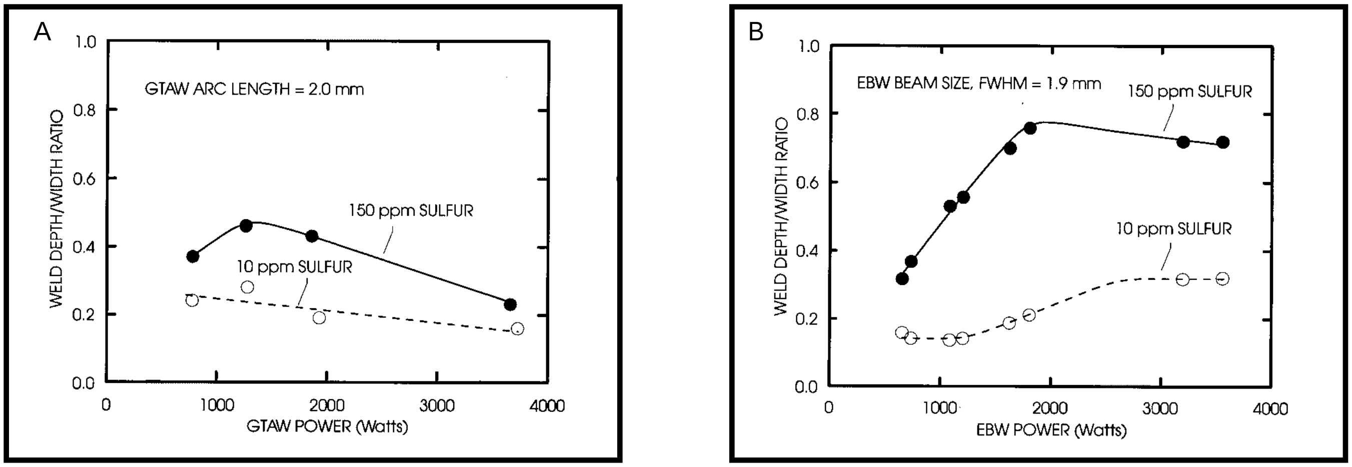

Fig. 7 — Weld D/W ratios for GTA and similar EB welds made on low- and high-sulfur material. A — GTA weld D/W ratios vs. arc power for fixed arc length; B — EB weld D/W ratios vs. beam power for fixed beam size.

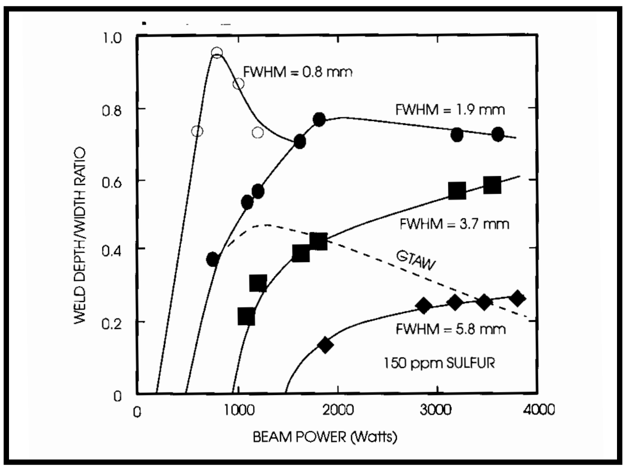

Fig. 8 — EB weld D/W ratios vs. beam power for welds made at various beam sizes on the high-sulfur material. Also shown is a line showing the D/W ratios for similar GTA welds.

focus and increases nearly linearly up to beam sizes of at least $\sigma = 3$ mm.

To compare electron beam welds with arc (GTAW) welds, it is necessary to have equivalent information about the arc power input distribution. Measurements of spatial distribution of power density were not made for this study, but these measurements have been made in the past for arc conditions comparable to those utilized in this study. Most arc size data presented in the literature were obtained using a split anode apparatus (Refs. 16 and 17). In addition, Saedi and Unkel (Ref. 18) measured the plasma size using a photo-diode array, which presumably yields the arc current distribution. All these data are summarized in Fig. 2. Note, the data of Nestor (Ref. 17) were obtained at an arc length of 6.3 mm. Nestor's data were extrapolated to a more representative 2-mm arc length using the trend of decreasing arc size for decreasing arc length, as established by Tsai (Ref. 16); the extrapolated values appear on Fig. 2. Also appearing on Fig. 2 are the calculated arc sizes derived by Choo and Szekely (Ref. 5).

As can be readily seen from Fig. 2, there is roughly a factor of two variation in arc size measurements among the various experiments. The origin of these differences is not presently understood. Unfortunately, it is also not possible to ascertain which are the more realistic values. This discrepency makes it impossible to directly compare the GTA and the EB welds in a simple manner. Nevertheless, these data define the range of beam sizes required to span the range characteristic of arc welding. Electron beam size therefore varied from about FWHM = 2 to 6 mm. The data shown in Fig. 2 also suggest that the arc size increases by about 2 mm as arc power increases from 600 to 3600 W and that the arc size is a function of other welding variables, notably the arc length.

Material Selection and Preparation

To assist in separating arc from thermocapillarity effects, two heats of Type 304L stainless steel were used in this study. These two heats of steel were chosen for their distinctly different observed GTA welding penetration characteristics. Typical GTA weld cross sections for the two heats of steel were shown in Fig. 1. The 150 ppm sulfur material had a D/W value of 0.47 in a standardized GTA weld test, while the 10 ppm sulfur material had a D/W value of 0.22 in the same weld test. Aside from the difference in sulfur contents, these two heats of material have similar compositions.

Cylindrical weld coupons were machined from the two heats of material to a length of 114 mm and a diameter of 62 mm. The specimens were cleaned immediately before welding with alcohol and paper wipes. Several welds were then made circumferentially around each bar. To avoid preheating effects, the coupons were cooled to room temperature between welds.

GTA Welding Equipment

The GTA welds were made with a fixed position torch at top center above the horizontally positioned weld coupons. The arc length was fixed at a distance set prior to welding using a feeler gauge. A water-cooled torch with a 2.38-mm-diameter, 2%-thoriated tungsten electrode was used. The electrode was ground to a 10-deg included angle truncated to a 0.76-mm diameter. The electrode stickout was set to 25 mm so that the electrode protruded 12 mm past the gas cup. To minimize weld pool contamination and arc variations from a variable atmosphere, the GTA welding was performed inside a high purity argon gas filled glove box. The oxygen and water vapor content of the glove box was maintained below 50 ppm by volume. Argon shielding gas was also supplied through the welding torch at a flow rate of 7 L/ min. All welds were made with DCEN power from a 350-A maximum output GTAW power supply.

EB Welding Equipment

The electron beam welds were made with a 7.5-kW, high-vacuum type electron beam welding machine. In all cases, the welds were made at 100 kV of accelerating voltage. The beam power was varied by adjusting the beam current. Various beam size and power density conditions were created by varying degrees of beam overfocus. Welds were made by rotating the horizontally positioned weld coupons under the fixed-position electron beam. The gun-to-work distance was fixed at 152 mm.

GTA Weld Variable Matrix

In an effort to generate GTA welds that might reveal the effects of the arc forces, a wide range of weld currents and arc lengths was incorporated into the experimental design. A series of traveling autogenous GTA welds was made on both the high- and low-penetration heats of stainless steel. A full factorial statistical experimental design was utilized where the independent variables were the material composition, welding current and the arc length. There were four levels of weld current: 100, 150, 200 and 300 A. Three levels of arc length were used: 1.0,1.5 and 2.0 mm. In all cases, the travel speed was 127 mm/min.

EB Weld Variable Matrix

Weld variable selection for the EB welds was intended to match the conditions produced during the GTA welding. Power levels and arc power distribution widths were matched as well as possible. Thus, the independent variables for the EB welds were material composition, beam current and beam defocus. Beam current was adjusted to match the arc power level. Note that the process efficiency of electron beam is expected to be higher than that of the arc. Therefore, EB welds were made with beam power levels equal to and 10% less than the overall arc power (voltage times current). Beam defocus was varied between about 2 and 6 mm (FWHM). The travel speed was fixed at the same 127 mm/min and the beam voltage was fixed at 100 kV. Figure 3 shows the experimental matrix of EB welds used for this study. Also shown on Fig. 3 are experimentally observed boundaries for nonmelting and keyhole formation. Large beam defocus (low power density) yielded no melting, while small beam defocus (high power density) produced obvious keyhole formation.

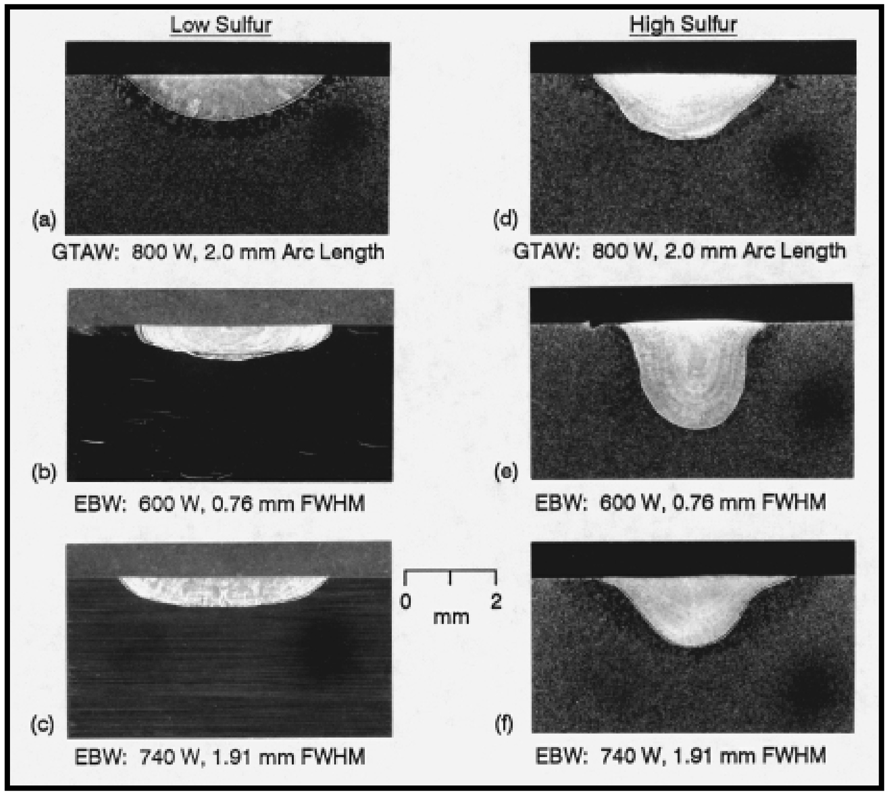

Fig. 9 — Cross sections of GTA welds made at 800 W on the high- and low-sulfur materials. Also shown are EB welds made at the same power and two beam sizes showing the similar shape of the GTA and the EB welds when the source size is properly matched.

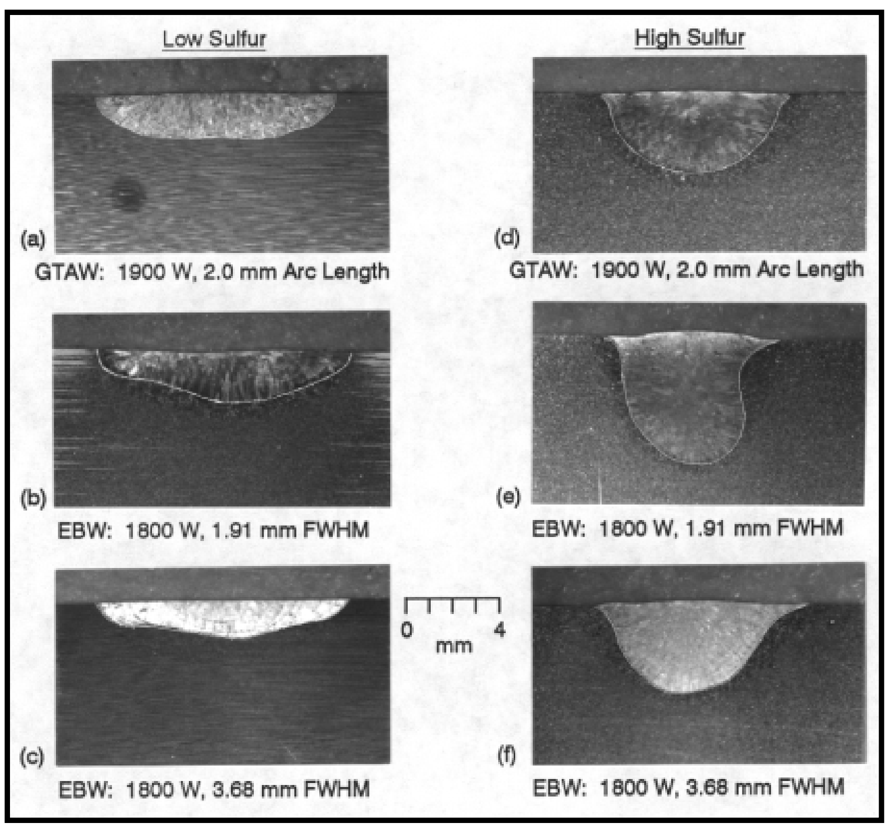

Fig. 10 — Cross sections of GTA and EB welds made at 1900 W on the high- and low-sulfur materials. Also shown are EB welds made at the same power and two beam sizes showing that a weld shape match between the GTA and the EB welds cannot be simply achieved at high power.

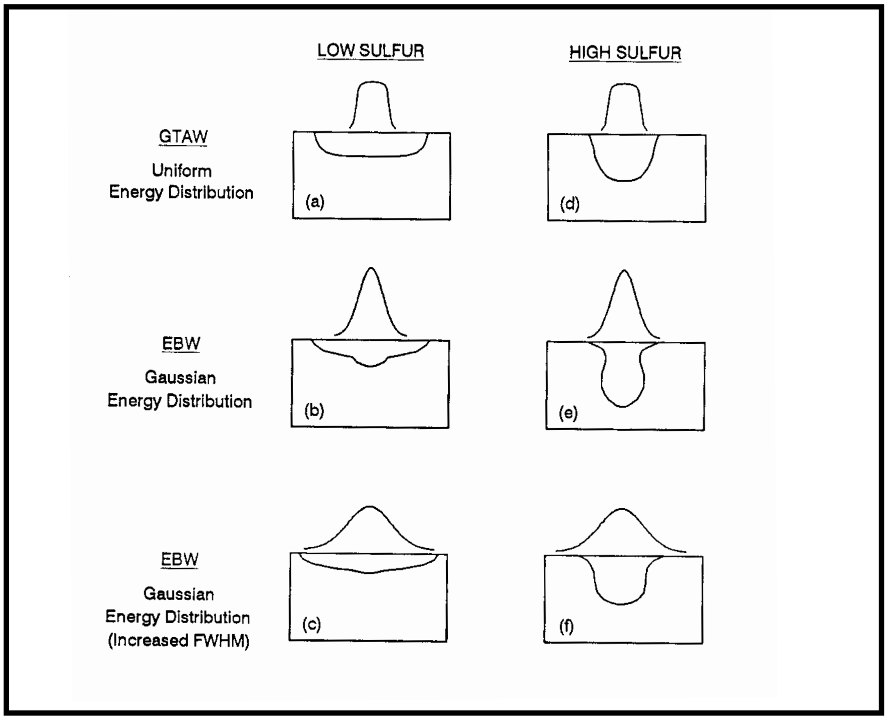

Fig. 11 — Typical observed weld shapes and their relationship to the known Gaussian EBW beam distribution and the proposed uniform GTAW arc distribution.

Results and Discussion

Weld Area

GTA welds were made on the two heats of material at a fixed travel speed of 127 mm/min with a wide range of arc length and arc power values. Cross-sectional areas of the weld nugget were computed from transverse metallographic sections of the welds. These data were combined with similar data available from previous studies of weld shape (Ref. 3) on the same materials. The weld cross-sectional area data are described by

$$A = 0.0027\frac{P^{1.3}}{v^{0.7}}\left(\frac{D}{W}\right)^{0.5} \quad \left(mm^2\right) \qquad (3)$$

where A is the weld cross-sectional area in mm^2; P is the arc power in Watts; ν is the travel speed in mm/s; and (D/W) is the weld depth-to-width ratio. Equation 3 is empirical, but it is based on theoretical expectations. Power law dependencies on P and ν were chosen because heat flow calculations suggest that these dependencies are the expected behavior. The factor related to weld depth-to-width ratio is entirely empirical but is qualitatively reasonable. A small D/W weld is equivalent to one where the input power is spread over a large surface area. In this case, heat is conducted away from the arc through a larger surface and a smaller melt volume will result. Larger D/W welds are nearer to the optimal surface-to-volume ratio of the weld pool and therefore have a larger melt volume. Figure 4 compares the experimental weld areas to the areas computed using Equation 3 and shows the quality of fit over a wide range of welding variables used.

Cross-sectional areas were also computed for the similar EB welds on the two heats of material. The EB welds are described by

$$A = 0.0033\frac{P^{1.3}}{v^{0.7}}\left(\frac{D}{W}\right)^{0.5} \quad \left(mm^2\right) \qquad (4)$$

Equation 4 was derived using Equation 3 as a starting point. Figure 5 shows the measured areas of the EB welds, generated with beam sizes ranging from FWHM = 1.9 to 4.6 mm. The curves drawn on Fig. 5 were generated using Equation 4.

Equations 3 and 4 are good evidence that the GTA and EB welds are similar in overall size and react nearly the same to changes in the welding variables. The different constants on Equations 3 and 4 imply that the process efficiency of GTA is about 82% that of EB.

Weld Shape

Since the thermocapillary effects of interest to this study are mainly manifested in weld shape, a simple indicator of weld shape is needed. For this study, weld depth-to-width ratio, D/W, is used as the shape indicator. D/W values were calculated from transverse metallographic cross sections of the welds. The D/W values of the GTA welds on the two heats of material are shown in Fig. 6A as a function of arc length (for the GTA process, source size should be proportional to the arc length). Notice that the D/W ratio values decrease monotonically with increasing source size for the high-sulfur material and that the D/W values are essentially constant for the low-sulfur material. This behavior is similar to that reported previously by Burgardt and Heiple (Ref. 12). Electron beam welds made at the same power and with increasing beam size show behavior similar to the GTA welds.

The D/W ratios for these EB welds are shown in Fig. 6B. A comparison of the data in Fig. 6A and 6B confirms that weld shape is largely controlled by thermocapillary effects for both arc and nonarc processes. The dependences of weld D/W ratio on increasing heat source size are a result of the interplay of weakened fluid flow and widening of the weld, caused by the broadened heat source distribution. Because of this interplay, it is reasonable that the high-sulfur welds would show a large decrease in weld D/W (weakened fluid flow and weld widening tend to reinforce each other) while the low-sulfur welds show a small change in D/W (weakened fluid flow tends to increase the D/W in competition with the weld widening).

If one assumes that the D/W values of the EB and GTA welds should be identical for the same heat source size, the arc size can be inferred from the EB weld data. Examination of the 150-ppm sulfur data on Fig. 6A and 6B shows that the heat source size for a 1-mm arc length is probably about FWHM = 1.9 mm. The arc size apparently increases monotonically to about FWHM = 2.5 mm as the arc length is increased to 2.0 mm. These inferred values of arc size are reasonable when compared to measured values shown in Fig. 2. It is disconcerting to note that welds made on the 10-ppm sulfur material are not consistent with this analysis. The EB welds on low-sulfur material always exhibited a smaller D/W value than those made with the GTA process. This difference in behavior between the high- and low-sulfur material persists for all data presented here and is not fully understood.

Welds made with the GTA process, at a fixed arc length of 2 mm, were produced on the two heats of material as a function of arc power. The D/W values measured from these welds are shown in

Fig. 7A. Notice that the D/W ratio values pass through a maximum at about 1400 W for the high-sulfur material and that the D/W values are essentially constant for the low-sulfur material. This behavior is similar to that reported previously by Burgardt and Heiple (Ref. 12), and it was attributed to flow reversal at the higher arc power. Electron beam welds made at the same travel speed and with a beam size of FWHM = 1.9 mm should be comparable to the low power GTA welds. The D/W ratios for these EB welds are shown in Fig. 7B as a function of EB power. The fact that the EB and GTA welds show somewhat similar shape changes with increasing power again demonstrates that thermocapillary effects are qualitatively similar in arc and nonarc processes.

Clearly, the EB and GTA weld D/W ratio values shown in Fig. 7 are substantially different in magnitude. The EB weld D/W ratio values are consistently about twice as large as those obtained with the GTA process for similar power levels. (Note that the conduction-mode EB process should be quite useful in a sorting test used to establish the weldability of materials.) A possible explanation for the difference in D/W values between EB and GTA welds is that the heat source sizes were not matched properly (*i.e.,* the GTA heat source size is not constant with power). Also, the difference in D/W values between the processes may be a manifestation of the complexities produced by arc effects in the GTA process.

To help understand the effects of different heat source sizes, EB welds were made as a function of beam power with varying beam size from FWHM = 0.8 to 5.8 mm. Figure 8 shows the EB weld D/W ratio data. Weld D/W ratios from these variable beam size welds were compared with the D/W ratios of the arc welds (shown as the dashed line on Fig. 8) to find the best agreement and thereby to infer the arc sizes for the GTA welds. It is reasonable to suppose that the EB and GTA weld D/W ratios will be equal for a given power level when the heat source sizes are the same. Thus, arc width can be determined from Fig. 9 as points where the GTAW data line crosses an EBW data line. The arc size, inferred from analysis of the welds on the 150-ppm sulfur material, increases nearly linearly from about 1.9 mm at 600 W of arc power to about 5.8 mm at 3600 W of arc power. The apparent arc size dependence on power level is reasonable and is qualitatively similar to that determined by direct measurements. A similar analysis of the welds made on the 10-ppm sulfur material yields somewhat different results. The 10-ppm sulfur material welds followed a similar trend of arc size vs. power level. However, the inferred arc size for the low-sulfur material is consistently about 1 mm smaller than that of the high-sulfur material.

A difficulty with the computed heat source sizes is that they are larger at high power than the experimental measurements of arc size lead us to expect. That is, the heat is moved around or within the weld pool such that the arc welds are wider and shallower than expected for a particular arc heat input distribution. The cause of this arc weld widening phenomenon must be a mechanism that acts in the plasma of the arc but does not occur in vacuum. A likely candidate for this phenomenon is arc jet motion of gas in the arc plasma that can push liquid metal in the weld pool away from the arc center. This effect is called plasma shear force and it gives an outward weld pool flow that makes the arc welds wider and shallower. Obviously, plasma shear cannot occur in a vacuum and therefore is not present in the electron beam welds. If plasma shear is an important effect, the electron beam size must be increased above the real arc size to artificially create conditions somewhat like those created by the outward plasma motion.

One interpretation of the decrease in GTA weld D/W ratio with increasing power, above about 1500 W, for the high-sulfur material is simply that the arc size increases substantially. This explanation means that the thermocapillary flow reversal postulated by Burgardt and Heiple (Ref. 12) need not be invoked to explain the D/W ratio decrease observed in the high-power GTA welds. It is important to notice that thermocapillary flow reversal probably does occur under some conditions. Consider the FWHM = 0.8 mm data shown in Fig. 8, for example. The EB weld D/W ratio, as a function of beam power, is observed to pass through a maximum for a fixed heat source size. Thermocapillary flow reversal at a power density of about 1600 W/mm^2 is a reasonable explanation for that behavior. An interesting observation made in the course of this work is that thermocapillary flow reversal behavior was invariably accompanied by some keyhole penetration (this was most apparent in the shallower low-sulfur welds). This situation means that the material under the beam is approaching the boiling point when flow reversal occurs. These temperatures are probably not achieved in normal arc welding processes. It appears likely that arc processes do not have sufficient power density to make the weld pool surface hot enough to cause thermocapillary flow reversal except possibly under extreme conditions (very short arc lengths, for example).

To this point weld shape has been considered only in terms of the D/W ratio. This approach is satisfactory in general terms but a detailed consideration of weld shape is also useful. Figure 9 shows cross sections of the low- and high-sulfur GTA welds made at 800 W and an arc length of 2 mm. Notice that a reasonably good shape match is possible with an EB weld made at comparable power and beam size of FWHM = 1.9 mm (the same result as derived from Fig. 8). Figure 10 shows the GTA welds made at 1900 W and 2-mm arc lengths. It is apparent that a good shape match for both material types requires substantially different source sizes. Specifically, a good match occurs for the high-sulfur material with a source size of FWHM = 3.7 mm, but a source size of about FWHM = 1.9 mm is needed for the low-sulfur material.

Another complication is that the high power GTA welds actually have no counterparts in the EB welds. In all cases, the GTA welds are a bit more “rectangular” in shape and do not have the “wings” of melting extending to a considerable width. By examining all the weld cross sections, it seems reasonable to conclude that at least some of these difficulties are caused by a non-Gaussian arc shape. Presumably the arc has a nearly constant power density over much of its diameter. The proposed heat distribution shape is illustrated in Fig. 11A and 11D. This assumes heat distribution shape is consistent with direct measurements of arc shape, for example Nestor (Ref. 17). Figure 11B and 11E illustrate the weld shape that results from a Gaussian heat input. Notice that the weld D/W ratios are too large in this case. If the Gaussian input FWHM is increased substantially, the weld D/W values can be approximately duplicated but the GTA weld shape is not reproduced. This is illustrated in Fig. 11C and 11F. The origin of such a rectangular arc heat distribution is not fully understood, but it is likely that complex arc phenomena, such as plasma shear, distribute the arc heat in this manner.

The detailed shape of the arc may be more important in determining weld shape than has generally been recognized in the past. It is also possible that the non-Gaussian shape of the arc heat distribution accounts for the considerably different EB heat source size required to match the high- and low-sulfur GTA welds. Since the electron beam is Gaussian and the arc apparently is not, the EB conditions required to give a reasonable shape match to the GTA welds may be misleading.

Conclusions

It is difficult to experimentally separate normal conduction and fluid flow effects from more complex arc effects in the gas tungsten arc process. Therefore, welds were made with a nonarc process with constant heat source size to simulate the GTA welds and thereby infer what arc effects are occurring. Electron beam welding was used because the beam size can be readily adjusted to a constant value comparable to the arc size, the beam size is easily measured and the power is continuously variable over the range necessary to reproduce GTA welding conditions.

The GTA and EB welds are qualitatively similar, when made with comparable welding variables, thus demonstrating that thermocapillary flow and normal conduction are the dominant factors in determining weld pool shape. The similarity of the GTA and EB welds is also further proof that a more concentrated heat source substantially improves weld penetration in good penetration (high-sulfur) material but has little effect in low penetration (low-sulfur) material. However, substantial differences between GTA and EB weld shapes do occur, especially at high power. These detailed differences show that other arc-related factors are also important.

By matching the weld D/W ratio values achieved with the GTA and EB processes, it is possible to infer the arc size for a particular set of welding variables. This methodology was used to infer what arc factor changes accompany arc power increases. The most important arc factor appears to be a substantial increase in arc size that occurs with increasing arc current. The maximum in weld D/W ratio as a function of arc power that typically occurs for high-sulfur material appears to be a result of this substantial change in arc size. This information indicates that thermocapillary flow reversal probably does not occur in most GTA welds.

The inferred arc size increase with arc power is considerably larger than what direct measurements of arc size have shown. It is possible that the difference is related to gas motion in the arc plasma. Arc jet flow may induce fluid flow in the weld pool (plasma shear flow) so that the weld will become wider than the size of the arc alone would create. Plasma shear fluid flow, at 300 A of arc current, apparently causes a weld width increase equivalent to about an additional 2 mm of heat source size.

Differences in shape between the GTA and EB welds indicate the arc heat source is probably not Gaussian. The EB welds are made with a Gaussian heat source and show a rounded weld root shape with "wings" of melting at the top surface that are substantially wider than the bulk of the melt zone. Equivalent GTA welds have a more flattened weld root without the "wings" of melting. This demonstrates that the arc heat source is not Gaussian and probably is a rectangular distribution. The non-Gaussian shape of the arc may account for the fact that the same set of EB conditions cannot properly mimic both the low- and high-sulfur material welds. Arc shape appears to be important in determining the weld width and depth (detailed weld shape).

Acknowledgments

We are pleased to acknowledge the support of the U. S. Dept. of Energy, EG&G Rocky Flats and Los Alamos National Laboratory. This research was performed under DOE contract number DE-ACO4-90RF62349.

We also wish to thank the staff of the EG&G Rocky Flats Welding and Joining Department for their help and support in this work.

References

1. Heiple, C. R., and Roper, J. R. 1982. Mechanism for minor element effect on GTA fusion zone geometry. *Welding Journal* 61(4): 97-s to 102-s.
2. Mills, K. C., and Keene, B. J. 1990. Factors affecting variable weld penetration. *International Materials Review* 35: 185–216.
3. Choo, R. T. C., and Szekely, J. 1992. Vaporization kinetics and surface temperature in a mutually coupled spot gas tungsten arc weld and weld pool. *Welding Journal* 71(3): 77-s to 93-s.
4. Choo, R. T. C., and Szekely, J. 1991. The effect of gas shear stress on Marangoni flows in arc welding. *Welding Journal* 70(9): 223-s to 233-s.
5. Choo, R. T. C., and Szekely, J. 1990. Modeling of high-current arcs with emphasis on free surface phenomena in the weld pool. *Welding Journal* 69(9): 346-s to 361-s.
6. Kim, S. D., and Na, S. J. 1992. Effect of weld pool deformation on weld penetration in stationary gas tungsten arc welding. *Welding Journal* 71(5): 179-s to 193-s.
7. Tsai, M. C., and Kou, S. 1990. Electromagnetic-force induced convection in weld pools with a free surface. *Welding Journal* 69(6): 241-s to 246-s.
8. Zacharia, T., David, S. A., Vitek, J. M., and DebRoy, T. 1989. Weld pool development during GTA and laser beam welding of Type 304S S, part 1—theoretical analysis. *Welding Journal* 68(12): 499-s to 509-s.
9. Rokhlin, S. I., and Guu, A. C. 1992. A study of arc force, pool depression and weld penetration during gas tungsten arc welding. *International Trends in Welding Science and Technology*, pp. 725–730, ASM International, Materials Park, Ohio.
10. Matsunawa, A., and Yokoya, S. 1989. Fluid flow and its effect on penetration shape in stationary welds. *Recent Trends in Welding Science and Technology*, pp. 31–35, ASM International, Materials Park, Ohio.
11. Oreper, G. M., Eagar, T. W., and Szekely, J. 1983. Convection in arc weld pools. *Welding Journal* 62(11): 307-s to 312-s.
12. Burgardt, P., and Heiple, C. R. 1986. Interaction between impurities and welding variables in determining GTA weld shape. *Welding Journal* 65(6): 150-s to 155-s.
13. Burgardt, P. 1992. Welding variable effects on weld shape in electron beam welding of stainless steels. *Engineering Materials*, pp. 269–328, Trans Tech Publications, Zurich, Switzerland.
14. Heiple, C. R., Roper, J. R., Stagner, R. T., and Aden, R. J. 1983. Surface active element effects on the shape of GTA, laser and electron beam welds. *Welding Journal* 62(3): 72-s to 77-s.
15. Burgardt, P. 1989. Evaluation of modified Faraday cup. Report No. RFP-437I, Internal Report of EG&G Rocky Flats, Golden, Colo.
16. Tsai, N. 1983. Heat distribution and weld bead geometry in arc welding. Ph.D. thesis, Massachusetts Institute of Technology, Boston, Mass.
17. Nestor, O. H. 1962. Heat intensity and current density distributions at the anode of high current arcs. *Journal of Applied Physics* 33: 1638–1648.
18. Saedi, H. R., and Unkel, W. 1988. Arc and weld pool behavior for pulsed current GTAW. *Welding Journal* 67(11): 247-s to 255-s.